Nanoscale

Accepted Manuscript

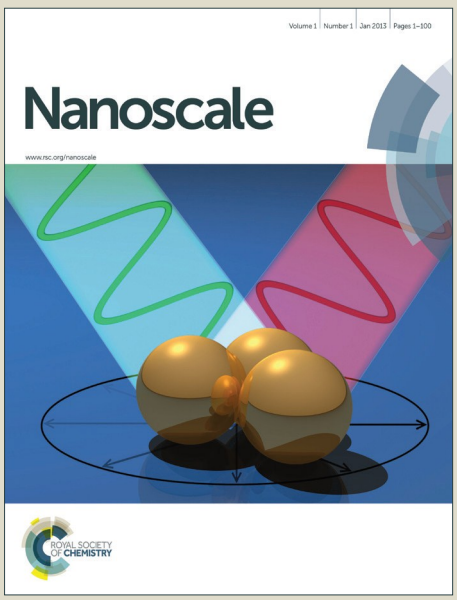

ROYAL SOCIETY OF CHEMISTRY

www.rsc.org/nanoscale

Nanoscale

ARTICLE

Rapid Synthesis of Hybrids and Hollow PdO Nanotructures by Controlled In-situ Dissolution of a ZnO Nanorod Template: Insights into the Formation Mechanism and Thermal Stability

Received 00th January 20xx,
Accepted 00th January 20xx

DOI: 10.1039/x0xx00000x

www.rsc.org/

Subhajit Kundu[a] and N. Ravishankar[a] *

Hollow nanomaterials have attracted a lot of interest by virtue of their wide range of applications that arise primarily due to their unique architecture. A common strategy to synthesize hollow nanomaterials is by nucleation of the shell material over a preformed core and subsequent dissolution of the core in the second step. Herein an ultrafast, microwave route has been demonstrated, to synthesize PdO nanotubes in a single step using ZnO as sacrificial template. The mechanism of the nanotube formation has been investigated in detail using control experiments. By tuning the starting ratio of $PdCl_2$:ZnO, hollow to hybrid PdO nanostructures could be obtained using the same method. Conversion of the PdO to Pd nanotubes has been shown by simple $NaBH_4$ treatment. Thermal stability of the PdO nanotubes have been studied. The insights presented here are general and applicable for the synthesis of hybrids/hollow structures in other systems as well.

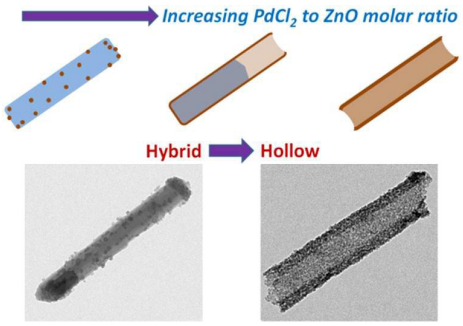

Introduction

Development of nanomaterials with high surface to volume ratio with sufficient stability is important for several applications.[1-14] Hollow nanomaterials have been investigated extensively in that regard. Various strategies have been reported in literature for synthesis of hollow nanomaterials viz. template-directed growth, directed assembly and electrochemical anodization.[15-21] Among these methods, the use of sacrificial templates has been a favored method to synthesize hollow nanomaterials. Examples include the use of silica, anodic alumina, polycarbonate and carbon nanotubes as templates for synthesis of various hollow metal nanostructures.[22-24] Recently, Se and Ag nanowires have been used as templates to synthesize various metal nanotubes.[25-28] Some of these methods use rather expensive sacrificial nanostructures and the dissolution of the templates are often difficult and time consuming.

ZnO[29, 30] is an inexpensive, sacrificial template specially for synthesis of various 1-D hollow nanostructures due to its crystallographically favourable rod/wire morphology along with easy dissolution in acidic/alkaline condition. Recently, ZnO sacrificial templates have been shown to promote hydrolysis of salts (to form the shell material) by simultaneous dissolution.[15] Such a phenomenon offers a distinct advantage of synthesis of various hollow nanomaterials in a single step and hence been exploited largely to synthesize various metal/metal oxide nanotubes for varied applications.[31-35] A detailed understanding of the mechanism of nucleation and dissolution is crucial to control the nature of the product. Here, using PdO as a model system, we have carried out detailed control experiments to elucidate the mechanism and gain understanding of the critical parameters for nanotube formation. Using these insights, we show that it is possible to form hollow PdO nanotubes or ZnO-PdO hybrids. The PdO could be easily converted to Pd nanotubes by simple $NaBH_4$ solution treatment leading to the formation of ZnO-Pd hybrids or hollow Pd thus dramatically increasing the range of nanostructures that can be obtained using the same method. We also have carried out in-situ TEM studies to investigate the thermal stability of the nanotubes that is critical for applications.

Experimental

Synthesis of ZnO nanorods:

ZnO nanorods have been synthesized by literature method.[36, 37] 29.5 mg of $ZnAc_2$ is dissolved in 125 ml of methanol by stirring in a beaker. The beaker is placed in an oil bath to attain a temperature of 65°C. 14.8 mg of KOH is dissolved in 65 ml

[a] Materials Research Centre, Indian Institute of Science, Bangalore 560012 India.
Electronic Supplementary Information (ESI) available: Details of experiments conducted, additional TEM, SEM images and XRD data. See DOI: 10.1039/x0xx00000x

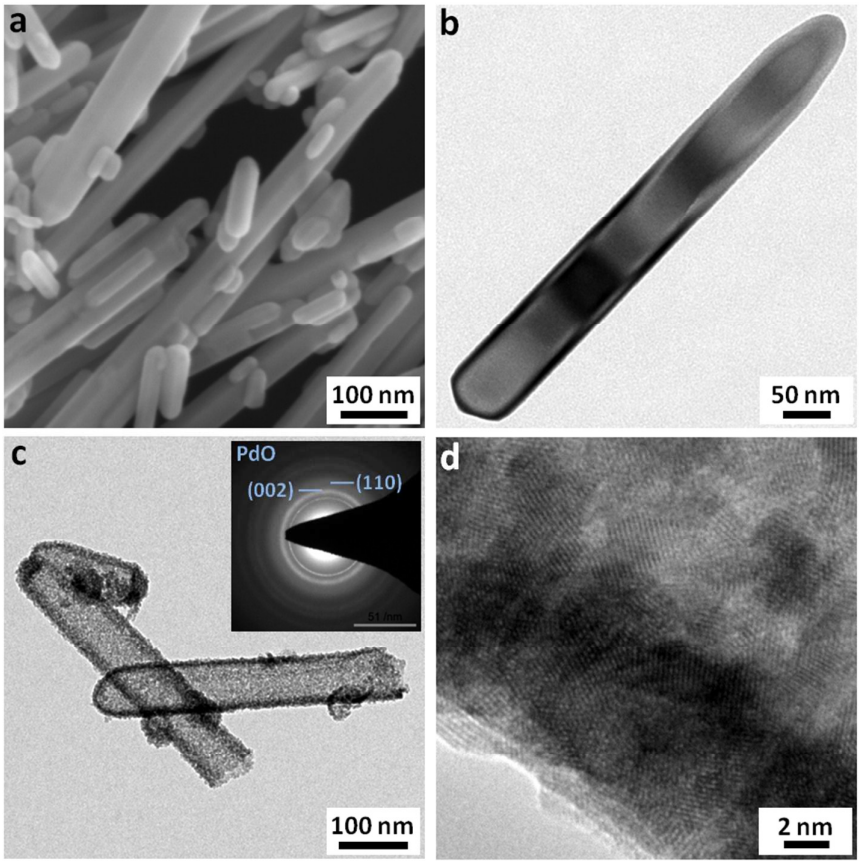

Figure 1. (a) SEM image of as-synthesized ZnO nanorods. (b) High magnification TEM image of a typical ZnO nanorod. (c) TEM image showing test tube-like and capsule-like PdO nanotubes. Diffraction pattern in the inset shows that the nanotubes are constituted of a large number of randomly oriented fine crystals of PdO. (d) HR-TEM image showing random orientation of the constituent PdO crystals.

of methanol in a separate beaker. The KOH solution obtained, is added to the stirring ZnO solution. The reaction is continued at 65°C till the volume of the solution becomes half. Then the solution in transferred to a Teflon container that is subsequently sealed inside a steel autoclave. The autoclave is kept in furnace at 120°C for 24 hours. The product is cooled and washed with water several times till the pH reaches ~7. The cleaned product is dried in oven before further use.

Synthesis of PdO nanorods/ZnO-PdO hybrids:

In a typical synthesis, 'x' mg of $PdCl_2$ (refer table 1) was dissolved/dispersed in 'v' ml of water by stirring for few minutes. 'w' mg of ZnO dispersed in 1 ml of water (by ultrasonication), was added to the stirring $PdCl_2$ solution. Microwave heating (maximum power 250 W) of the solution was done in closed vessel condition for 't' minutes at 'T'°C. The colour of the suspension turns dark from light brown. The synthesized nanomaterial was precipitated and the supernatant was collected for analysis. Precipitate was cleaned with deionized water several times and finally with acetone and left overnight for drying.

Table 1. Reactant amount and reaction condition for each sample.

Sample name	ZnO 'w' (mg)	$PdCl_2$ 'x' (mg)	H_2O 'v' (mg)	temp. 'T' (°C)	time 't' (min)
ZP-1	20	20	6	200	5
ZP-2	20	10	6	200	5
ZP-3	10	2.5	18	100	5
ZP-4	20	25	6	200	5
ZP-5	20	20	6	200	20
ZP-6	20	20	6	100	5
ZP-7	20	20	6	26	5

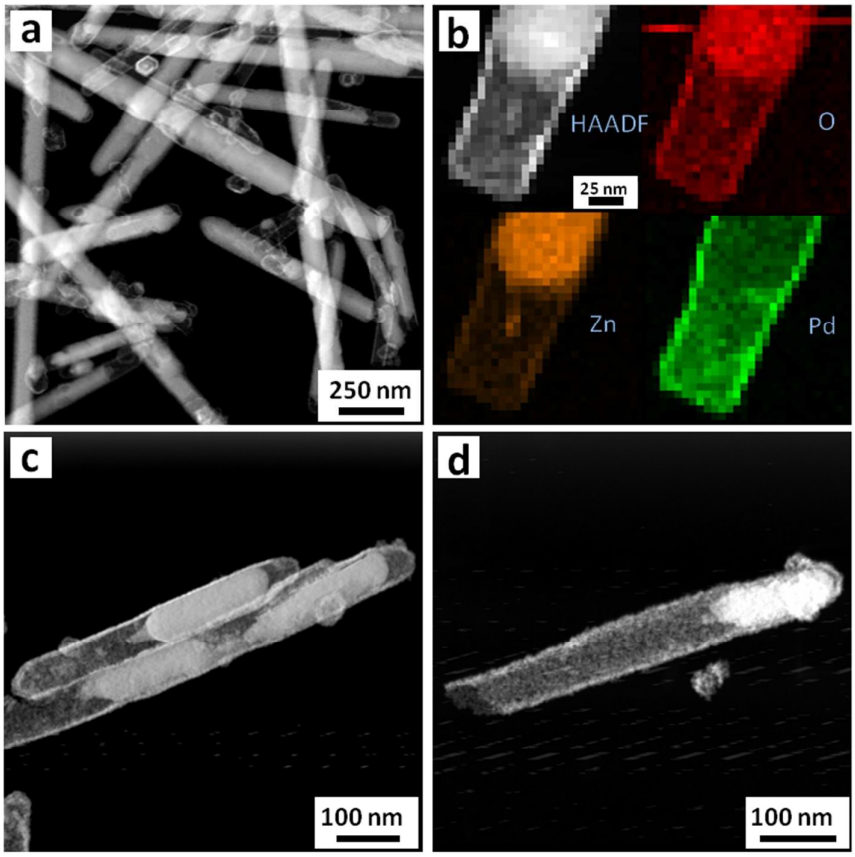

Figure 2. (a) Low magnification HAADF STEM image showing that the dissolution of ZnO is suppressed at lower $PdCl_2$:ZnO ratio. (b) HAADF STEM image with EDS maps from the tip of a partially etched nanorod showing the distribution of the different elements present. (c) A case where dissolution has happened through the pores in the caps. (d) Higher rate of dissolution leads to opening of tubes from one/both end in some cases.

RESULTS AND DISCUSSION

The as-grown ZnO nanorods (wurtzite phase) have a hexagonal prismatic morphology as indicated by the SEM micrograph (Figure 1a). The nanorods have a diameter of about 20-90 nm with variable length from about few tens of nm to about a micron. Figure 1b show high magnification TEM image of a typical ZnO nanorod. Figure 1c shows the bright-field transmission electron microscope (TEM) image of the as-synthesized PdO nanotubes (ZP-1). Three kinds of tubes are identified – capsule-like, test-tube like and pipe-like. Careful observation reveals the grain structure of the nanotubes. Electron diffraction from individual nanotubes show very broad rings corresponding to PdO phase implying that the tubes are constituted of very fine crystals of PdO randomly oriented. The high-resolution TEM image in Figure 1d show random orientation of the constituent PdO nanoparticles. Few of the PdO nanotubes contain residual amount of undissolved ZnO inside. This possibly indicates that the hollow nanotubes of PdO formed by nucleation on the pre-existing ZnO nanorods that acts as a sacrificial template. X-ray diffraction (XRD) pattern (Supporting Information, Figure-S2c) of the powder sample shows broad peaks corresponding to (002), (110), (102), (112), (103), (004) reflections representing the tetragonal phase of PdO (JCPDS - 850713). Calculation of the crystallite size of the constituent PdO nanoparticles from the broadening of (110) peak showed it to be ~3 nm. Low intensity peaks corresponding to ZnO is also seen consistent with the TEM observations. Surface analysis of the powder by X-ray Photoelectron Spectroscopy (XPS) also show trace amounts of Zn along with Pd (Supporting Information, Figure-S2d, e). High resolution scan around the Zn 2p peak show only one set of peak corresponding to the +2 oxidation state in the oxide. Pd 3d XPS spectrum shows the presence of +2 oxidation state of Pd predominantly (Pd 3d5/2 peak at ~336.9 eV) due to the oxide.[38] A small peak at ~338.5 eV is also present which could be due to trace amounts of oxide of Pd with a higher oxidation state.[39] No detectable peak for metallic Pd could be identified.
To understand the reason behind formation of PdO from $PdCl_2$, the reaction has been carried out without the ZnO nanorods under similar conditions (ZP-1control). XRD analysis of the as-synthesized (uncleaned) product (Supporting Information,

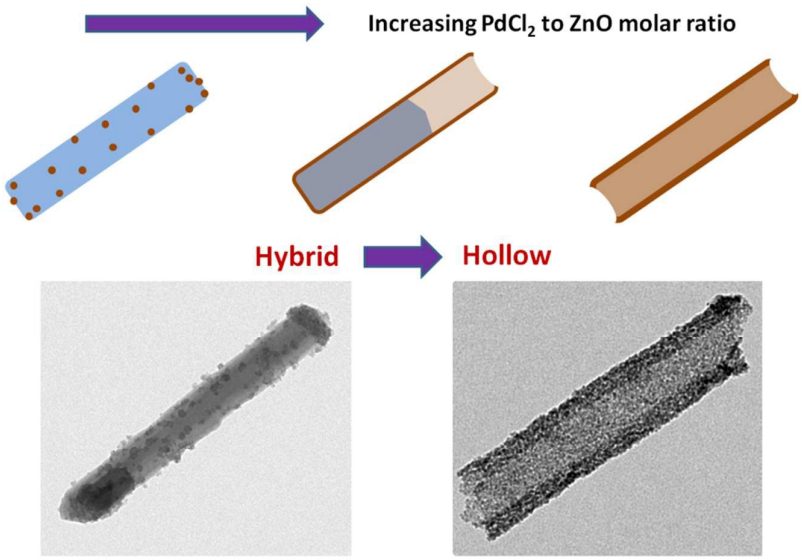

Figure 3. Schematic showing that low starting ratio of PdCl2:ZnO primarily yields PdO attached ZnO nanorods where as at high starting ratio of PdCl2:ZnO predominantly PdO nanotubes are obtained.

Figure-S3) show similar broad peaks of PdO along with sharp, small peaks of metallic Pd. Formation of trace amounts of Pd is possibly due to enhanced absorption of microwave by the $PdCl_2$ solution in absence of ZnO leading to reduction under excess superheating.[40] Few low angle, intermediate peaks could be identified indicating incomplete conversion of $PdCl_2$ to PdO/Pd under the reaction condition. Analysis of the pH of the supernatant show it to be ~1.4. Such extremely acidic pH on heating $PdCl_2$ in water could be due to generation of HCl as a result of its hydrolysis.

In-situ generation of HCl as a result of hydrolysis would depend on the starting amount of $PdCl_2$. Hence the reaction was carried out with half the amount of $PdCl_2$ keeping the amount of ZnO and water constant (ZP-2). XRD of the product (Supporting Information, Figure S4) shows higher amounts of ZnO relative to PdO which could be due to suppressed dissolution of ZnO. TEM investigation reveals that indeed the dissolution of ZnO has significantly reduced leading to higher number of partially etched nanorods compared to ZP-1. This implies that the HCl generated causes the dissolution of the ZnO nanorods.

For a better insight into the mechanism of dissolution, imaging (ZP-2) has been done in STEM mode which offers unambiguous thickness and/or atomic number contrast compared to the TEM mode. Low magnification HAADF-STEM image in figure 2a clearly show partial dissolution in majority of the nanorods. Imaging at higher magnification along with EDS mapping (Figure 2b) clearly reveals the morphology of the partially etched ZnO nanorods within the PdO shell. It is observed that etching primarily starts from the pores (Figure 2c, capsule-like) and in some cases due to higher rate of dissolution it leads to opening of one of the tips (Figure 2d, test-tube like) resulting in faster etching from one side than the other. In extreme of cases such a process gets initiated from both ends resulting in pipe-like nanotubes.

To further lower the dissolution of ZnO, an experiment has been carried out at further lower $PdCl_2$: ZnO molar ratio (ZP-3) with increased amount of water (to lower the post-hydrolysis pH further) at a lower temperature (Supporting Information, figure S5). Dissolution of ZnO is seen to be extremely suppressed giving rise to predominantly PdO nanoparticle attached ZnO nanorods (hybrid) with trace amounts of partially/completely etched nanorods. Calculation of the H^+ ion concentration from the amount of $PdCl_2$ and water used shows that it is just an order of magnitude lower as compared to the case where we get nanotubes as the dominant product (Supporting Information, table ST 1). To check the accuracy of calculation of H^+ ion concentration, it was back calculated from the supernatant pH of the corresponding control experiment without ZnO. A very good match could be obtained between the two values validating that indeed a nominal change in H^+ ion concentration drastically alters the final product formed – hybrid/nanotubes (Figure 3).

Formation of PdO onto ZnO at low loading (ZP-3) clearly shows a preference for nucleation over nanorods with a smaller diameter (Figure 4a). Also, it is observed that there is a preference of nucleation (for less populated nanorods) over the tip than that on the cylindrical surfaces. This is due to higher interfacial energy of the basal planes over the prism planes and hence the difference in the ZnO/PdO interfacial energies that leads to differences in efficiency of heterogeneous nucleation.[41] On slightly increasing the loading of PdO (ZP-2) we observe preferential dissolution of the nanorods with smaller diameter on which PdO nucleates (Figure 4b). As the loading is further increased (ZP-1), we observe that the larger diameter nanorods also start dissolving. Thus, it is clear that both nucleation of PdO and dissolution starts from the nanorods with the smallest

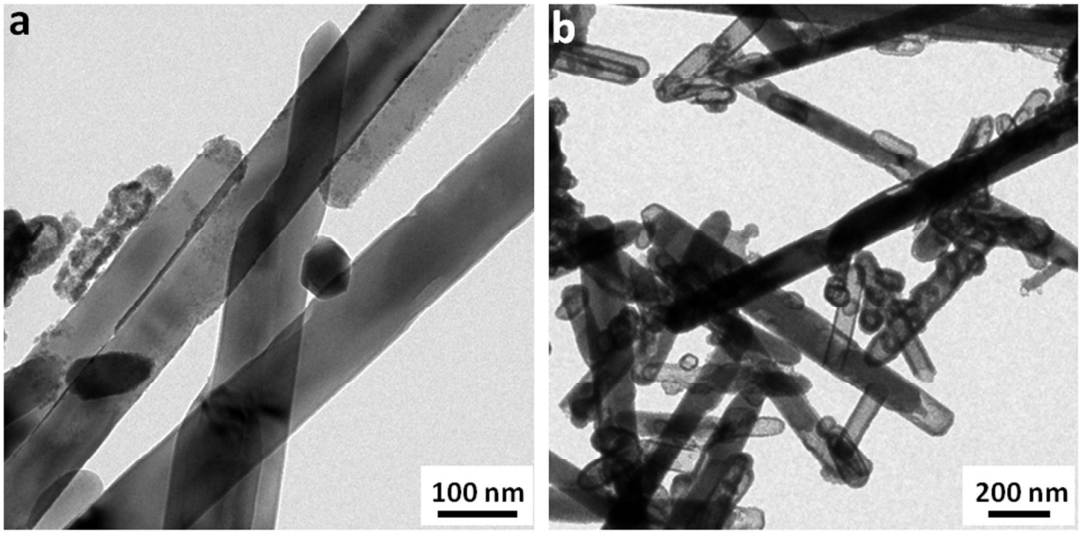

Figure 4. (a) At low loading (ZP-3), nucleation of PdO happens preferentially over nanorods with smaller diameter. Trace amounts of PdO nanotubes with smaller inner diameter and length is also found indicating preferential nucleation and dissolution. (b) As loading is increased (ZP-2) more of such nanotubes appear.

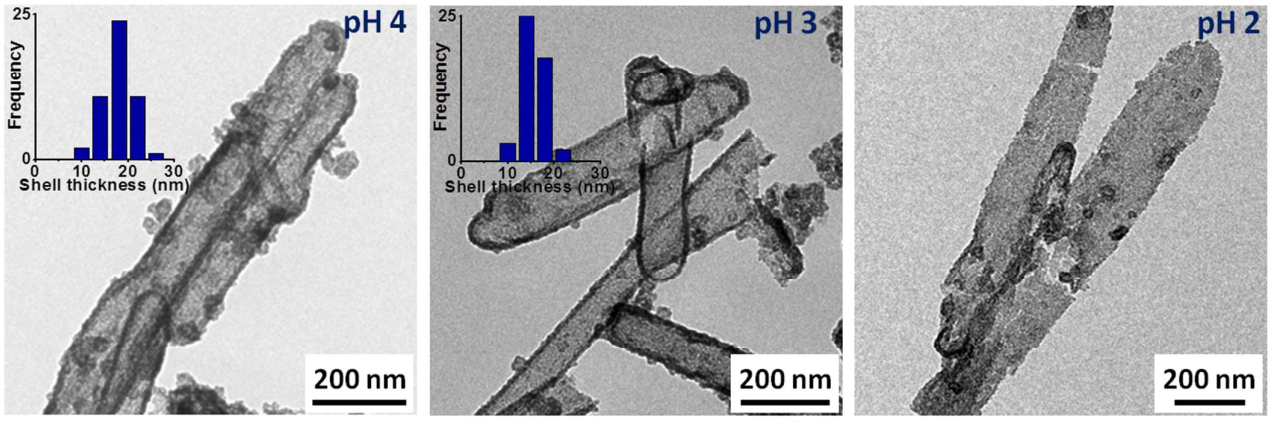

Figure 5. TEM images of HCl/H2O treated (different pH) PdO nanotubes (histogram of shell thickness is shown in the inset). Decreasing the pH leads to thinning of the shell which in the extreme case leads to opening of the nanotubes forming belt/sheet-like structures.

diameter and progresses to the larger diameter nanorods. This further reinforces the key role of interfacial energy as both the dissolution process and the nucleation process are favored in the smaller nanorods.[42, 43] The dissolution reaction takes up H^+ from the vicinity of the smaller diameter nanorods due to the reaction: $ZnO + 2H^+ \rightarrow Zn^{2+} + H_2O$. Such removal of H^+ promotes hydrolysis of $PdCl_2$ due to the reaction: $Pd^{2+} + 2H_2O \rightarrow Pd(OH)_2 + 2H^+$.[15] Therefore, the initial nucleation of PdO (as $Pd(OH)_2$ is unstable under the reaction condition) onto ZnO happens at the expense of partial dissolution of the nanorods about the diameter. Hence, smaller nanorods with higher solubility are preferred over bigger nanorods. Once a few layer of particles is formed, the dissolution from the sides slow down and hence the nucleation (shell thickness is nearly same for all nanotubes). Subsequent dissolution happen through the ends due to global pH of the solution. Incidentally, the nanorods which are smaller in diameter are also smaller in length due to which the smaller nanorods tend to completely dissolve off before the dissolution of the large nanorods.

At the highest $PdCl_2$:ZnO molar ratio we observed that still trace amount of the nanorods with bigger diameter remains undissolved. Dissolution of ZnO could be increased by increasing the amount of HCl generated. Hence the reaction was carried out at even higher $PdCl_2$:ZnO molar ratio (ZP-4). As expected, TEM investigation shows that the dissolution of the larger nanorods is increased in this case. However, significant side growth of PdO nanoclusters is observed to happen on the PdO nanotubes along with random aggregates outside. This could be due to poor solubility of $PdCl_2$ in water due to which the hydrolysis reaction happens progressively.

Ultra-small ZnO nanoparticles are known to undergo dissolution even at circumneutral pH. Therefore a final supernatant pH of 5.6 (ZP-1) could be enough to dissolve more of ZnO. Therefore the reaction was carried out for a longer time

(ZP-5). XRD data indicates that there is no significant decrease in the peak area of ZnO relative to PdO suggesting that at that pH, ZnO is stable.

Temperature may have an effect on the nucleation of the PdO nanoparticles onto ZnO and subsequent dissolution of the ZnO. To investigate this aspect, the reaction was carried out at different temperatures keeping all other parameters same. TEM images from sample prepared at 100˚C (ZP-6) show aggregated PdO nanoparticles forming outside the ZnO rod/template along with particles on it (Supporting Information, Figure S8). The particle size is bigger than samples prepared at 200˚C. Reaction carried out at room temperature (ZP-7) for extended time (2.5 hrs : as hydrolysis would be slow) shows even bigger particle size. However, XRD data of the samples show broadening of the PdO peaks with decreasing temperature implying reduction in crystallite size. Such a phenomenon is counterintuitive according to nucleation theory and may be understood by considering the solubility of the Pd precursor. $PdCl_2$ is sparingly soluble in water and its solubility decreases with temperature. Therefore at a lower temperature more of the precursor remains dissolved at any point of the reaction leading to a larger driving force for nucleation and hence a smaller grain size. Under these conditions, there is an enhanced chance for homogeneous nucleation in the solution phase along with heterogeneous nucleation on the ZnO nanorods and hence we observe the formation of clusters of PdO that are homogeneously formed in the lower temperature samples. However, the dissolution of ZnO rods was observed to be suppressed at a lower temperature. As the dissolution reaction is exothermic, such a phenomenon is expected due to purely kinetic reason.

In-situ dissolution of ZnO provides a very fast and efficient method to produce PdO nanotubes in large quantities. However, the shell thickness obtained was unique and is not controlled. Variation of $PdCl_2$:ZnO ratio does not alter the shell thickness. However, thinner shell would be more beneficial for applications requiring even more surface to volume ratio. Therefore, ex-situ dissolution study was carried out for making nanotubes with thinner PdO shell. In a typical reaction, the samples were stirred in a bath of HCl/H_2O tuned to a pH of ~4 for partial etching of PdO. TEM imaging (Figure 5) reveals removal of partially etched ZnO from inside the hollow nanotubes. Also, histogram of the shell thickness shows significant reduction under such treatment. At a pH of ~3 further etching happens leading to a thinning of the shell. This treatment also leads to a partial opening of the tubes in some cases. Further decreasing of the pH to ~2 lead to significant dissolution of the PdO nanotubes leading to formation of belt/sheet like structures due to opening of the nanotubes.

Nanostructures of Pd are specifically useful for several applications.[44-47] Therefore, to synthesize Pd attached ZnO nanorods, the reaction was carried out (lower loading) under additional presence of sodium citrate (Na_3Ct). XRD data of the hybrid (Supporting Information, Figure S10) indicates formation of Pd/PdO-ZnO hybrid as indicated by the XRD data. The peak corresponding to PdO is broad, as before, indicating

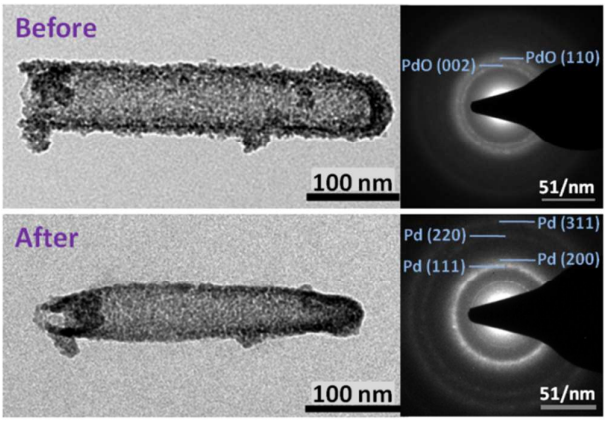

Figure 6. TEM images of a PdO nanotube before and after $NaBH_4$ treatment. Diffraction pattern alongside show that PdO reduces to Pd.

similar grain sizes but the peak for Pd is sharp indicating bigger crystallite size. TEM investigation also reveals inhomogeneously aggregated structures due to extreme sintering of Pd at high temperatures under microwave irradiation. Therefore, we understand that the thermal stability of the surfactantless Pd nanotubes in solution is rather poor and direct synthesis by the proposed one-pot method at high temperature under microwave radiation may not be ideal.

Reduction of PdO to Pd could be done at room temperature using stronger reducing agents. To test this hypothesis, PdO nanotubes were dispersed on to a TEM support membrane (PdO dispersion in acetone was dropcasted and dried). Imaging of PdO nanotube dispersed grid was done so as to mark the nanotubes to be studied. The same TEM support membrane was dipped in $NaBH_4$ solution for ~20 s to convert the PdO to Pd nanotubes. Figure 6 show the TEM images (Diffraction in the inset) of a single PdO nanotube before and after dipping into $NaBH_4$ solution. It is observed that PdO nanotubes immobilized on substrate could be converted to Pd nanotubes without major sintering at room temperature. Significant shrinkage of the diameter is observed on conversion to Pd nanotubes. Aggregated regions also showed similar stability. However, for scaling up, the same experiment was repeated by dispersing the nanotubes in aqueous solution. Addition of excess $NaBH_4$ solution to PdO nanotube dispersed solution at room temperature yielded pure Pd nanotubes as indicated by the XRD data (Supporting Information, figure S11). Broad peaks indicate that even in solution there has not been significant aggregation. TEM image along with electron diffraction further show that the grainy structure of individual tubes are maintained.

To investigate the thermal stability of the nanotubes, in-situ TEM study was carried out. The temperature of the TEM grid was increased in steps of 100˚C and at each temperature it was maintained for 20 mins. Figure 7 show TEM images of PdO nanotubes as it is heated to different temperature. It is observed that till 300˚C, the nanotubes showed no significant change in morphology and grain size. Beyond 300˚C, the grains started

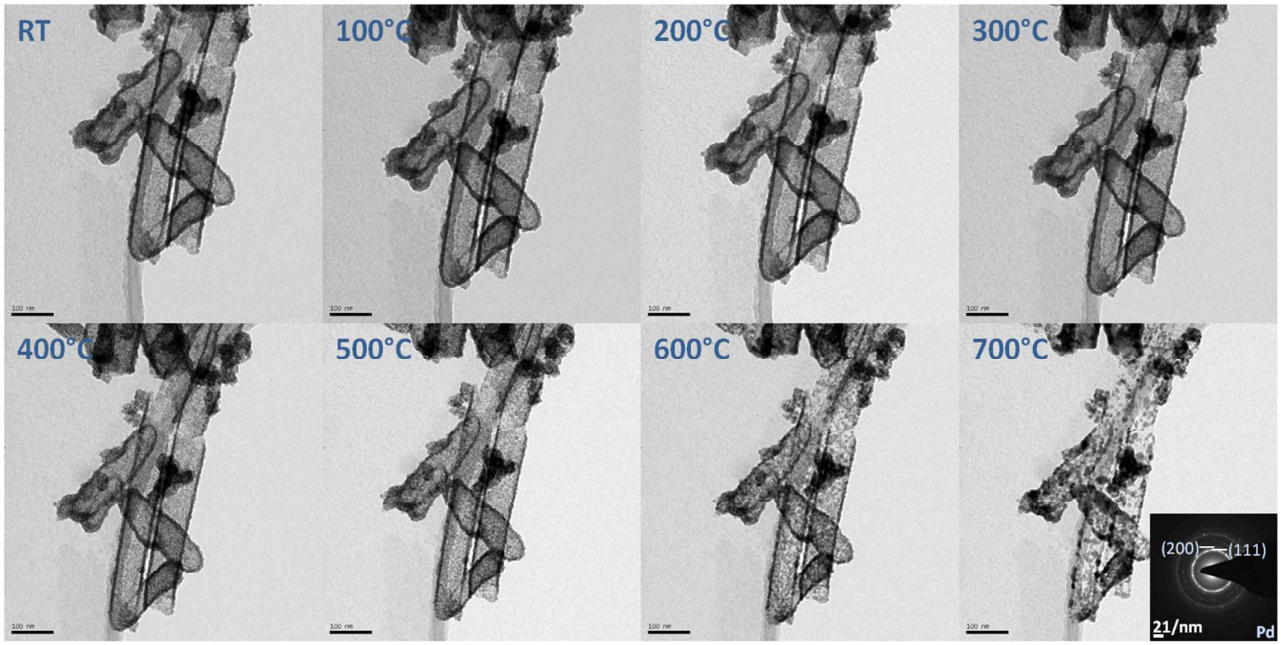

Figure 7. TEM images (Scale marker- 100 nm) of PdO nanotubes, showing the same region at different temperature. The nanotubes are seen to be stable till 300˚C. Above 300˚C the nanotube diameter and shell thickness start to shrink indicating onset of coalescence of the constituent grains. Diffraction in the inset show that above 700˚C the PdO nanotubes convert to Pd nanotubes.

coarsening resulting in thinning of the shell along with shrinkage of the diameter. Plot of the shell thickness and diameter with temperature confirms such a trend (Supporting Information, figure S12). The change in shell thickness and diameter is seen to be slow over time. But on increasing the temperature to 700˚C, a sudden coalescence of the constituent particles of the shell material was observed at which point the experiment was stopped by bringing down the temperature of the e-chip to room temperature. This sudden change could possibly be attributed to the conversion of PdO into Pd metal which is expected to have poorer thermal stability than the oxide. Electron diffraction from the nanotubes exposed/unexposed to electron beam confirmed the formation of Pd nanotubes. Such decomposition of PdO to Pd is known to happen at ~800˚C in air.[48] But we observe the decomposition at lower temperature inside the TEM probably due to lower oxygen partial pressure under vacuum. Therefore the thermal stability of the nanotubes is expected to be higher in air than estimated in this study.

Conclusions

In conclusion, we report an one-pot, ultrafast microwave route to synthesize PdO nanotubes in bulk. The mechanism of formation of nanotubes has been elucidated. Tuning the reaction condition suitably, ZnO-PdO hybrids could be obtained using the same method. The PdO nanotubes formed could be converted to Pd nanotubes in solution by simple $NaBH_4$ treatment. Thermal stability of the PdO nanotubes has been studied. The insights gained from the study has implication in tuning of the architecture/composition of the product based on the application required.

Acknowledgements

The authors acknowledge the Department of Science and Technology for funding. The Transmission Electron Microscopes and Aduro Protochips heating holder used, are part of the AFMM facility in IISc. Scanning Electron Microscope facility in CeNSE, IISc is acknowledged.

References

1. M. E. Davis, Nature, 2002, 417, 813-821.
2. H. K. Chae, D. Y. Siberio-Perez, J. Kim, Y. Go, M. Eddaoudi, A. J. Matzger, M. O'Keeffe and O. M. Yaghi, Nature, 2004, 427, 523-527.
3. S. H. Joo, J. Y. Park, C.-K. Tsung, Y. Yamada, P. Yang and G. A. Somorjai, Nat. Mater., 2009, 8, 126-131.
4. S. Yang and X. Luo, Nanoscale, 2014, 6, 4438-4457.
5. T. J. Barton, L. M. Bull, W. G. Klemperer, D. A. Loy, B. McEnaney, M. Misono, P. A. Monson, G. Pez, G. W. Scherer, J. C. Vartuli and O. M. Yaghi, Chem. Mater., 1999, 11, 2633-2656.
6. G. Chen, F. Rosei and D. Ma, Nanoscale, 2015, 7, 5578-5591.
7. E. A. Anumol, A. Halder, C. Nethravathi, B. Viswanath and N. Ravishankar, J. Mater. Chem., 2011, 21, 8721-8726.
8. X. Zhang, V. Thavasi, S. G. Mhaisalkar and S. Ramakrishna, Nanoscale, 2012, 4, 1707-1716.
9. L. Hu and Q. Chen, Nanoscale, 2014, 6, 1236-1257.
10. A. Halder, S. Patra, B. Viswanath, N. Munichandraiah and N. Ravishankar, Nanoscale, 2011, 3, 725-730.

11. R. Mukherjee, T. Chakrabarti, E. A. Anumol, T. A. Abinandanan and N. Ravishankar, ACS Nano, 2011, 5, 2700-2706.
12. S. Kundu, P. Kundu, G. V. Tendeloo and N. Ravishankar, Small, 2014, 10, 3895-3900.
13. S. Kundu, A. Leelavathi, G. Madras and N. Ravishankar, Langmuir, 2014, 30, 12690-12695.
14. E. A. Anumol, B. Viswanath, P. G. Ganesan, Y. Shi, G. Ramanath and N. Ravishankar, Nanoscale, 2010, 2, 1423-1425.
15. J. Liu, Y. Li, H. Fan, Z. Zhu, J. Jiang, R. Ding, Y. Hu and X. Huang, Chem. Mater., 2010, 22, 212-217.
16. H. J. Fan, U. Gösele and M. Zacharias, Small, 2007, 3, 1660-1671.
17. J. Wang and Z. Lin, Chem. Mater., 2008, 20, 1257-1261.
18. F. Caruso, R. A. Caruso and H. Möhwald, Chem. Mater., 1999, 11, 3309-3314.
19. F. Caruso, Chem. Eur. J., 2000, 6, 413-419.
20. L. Liu and S. Park, Chem. Mater., 2011, 23, 1456-1460.
21. S. Yu, U. Welp, L. Z. Hua, A. Rydh, W. K. Kwok and H. H. Wang, Chem. Mater., 2005, 17, 3445-3450.
22. C. R. Martin, Science, 1994, 266, 1961-1966.
23. P. M. Ajayan, O. Stephan, P. Redlich and C. Colliex, Nature, 1995, 375, 564-567.
24. S.-W. Kim, M. Kim, W. Y. Lee and T. Hyeon, J. Am. Chem. Soc., 2002, 124, 7642-7643.
25. Y. Bi and G. Lu, Chem. Mater., 2008, 20, 1224-1226.
26. Z. Chen, M. Waje, W. Li and Y. Yan, Angew. Chem. Int. Ed., 2007, 46, 4060-4063.
27. B. Mayers, X. Jiang, D. Sunderland, B. Cattle and Y. Xia, J. Am. Chem. Soc., 2003, 125, 13364-13365.
28. H.-W. Liang, S. Liu, J.-Y. Gong, S.-B. Wang, L. Wang and S.-H. Yu, Adv. Mater., 2009, 21, 1850-1854.
29. F. N. Meng, Y. Wang, P. Gao, G. L. Zhang, L. Q. Wang, G. R. Chen, S. Q. Yang and D. Bao, Adv. Mater. Res., 2012, 457, 815-818.
30. P. Gao, L. Wang, Y. Wang, Y. Chen, X. Wang and G. Zhang, Chem. Eur. J., 2012, 18, 4681-4686.
31. Y. W. Lee, M. A. Lim, S. W. Kang, I. Park and S. W. Han, Chem. Commun., 2011, 47, 6299-6301.
32. M. A. Lim, D. H. Kim, C.-O. Park, Y. W. Lee, S. W. Han, Z. Li, R. S. Williams and I. Park, ACS Nano, 2012, 6, 598-608.
33. B.-S. Choi, Y. W. Lee, S. W. Kang, J. W. Hong, J. Kim, I. Park and S. W. Han, ACS Nano, 2012, 6, 5659-5667.
34. Y.-j. Feng, L.-l. Liu and X.-d. Wang, J. Mater. Chem., 2011, 21, 15442-15448.
35. J. Liu, J. Jiang, M. Bosman and H. J. Fan, J. Mater. Chem., 2012, 22, 2419-2426.
36. C. Pacholski, A. Kornowski and H. Weller, Angew. Chem. Int. Ed., 2002, 41, 1188-1191.
37. A. Leelavathi, G. Madras and N. Ravishankar, Phys. Chem. Chem. Phys., 2013, 15, 10795-10802.
38. T. H. Fleisch, G. W. Zajac, J. O. Schreiner and G. J. Mains, Appl. Surf. Sci., 1986, 26, 488-497.
39. J. M. Tura, P. Regull, L. Victori and M. D. de Castellar, Surf. Interface Anal., 1988, 11, 447-449.
40. E. A. Anumol, P. Kundu, P. A. Deshpande, G. Madras and N. Ravishankar, ACS Nano, 2011, 5, 8049-8061.
41. P. Kundu, N. Singhania, G. Madras and N. Ravishankar, Dalton Trans., 2012, 41, 8762-8766.
42. S.-W. Bian, I. A. Mudunkotuwa, T. Rupasinghe and V. H. Grassian, Langmuir, 2011, 27, 6059-6068.
43. E. A. Meulenkamp, J. Phys. Chem. B, 1998, 102, 7764-7769.
44. L. Schlapbach and A. Zuttel, Nature, 2001, 414, 353-358.
45. G. Li, H. Kobayashi, S. Dekura, R. Ikeda, Y. Kubota, K. Kato, M. Takata, T. Yamamoto, S. Matsumura and H. Kitagawa, J. Am. Chem. Soc., 2014, 136, 10222-10225.
46. W. R. Schwartz and L. D. Pfefferle, J. Phys. Chem. C, 2012, 116, 8571-8578.
47. C. Bianchini and P. K. Shen, Chem. Rev. (Washington, DC, U. S.), 2009, 109, 4183-4206.
48. R. J. Farrauto, J. K. Lampert, M. C. Hobson and E. M. Waterman, Appl. Catal., B, 1995, 6, 263-270.